EPR probe study of the molecular dynamics of the supercooled liquid, the glass state, and the glass transition in liquid-crystalline MBBA [*n*-(*p*-methoxybenzlidene)-*p*-butylaniline]

Johanan Isaac Spielberg and Edward Gelerinter*
Physics Department and Liquid Crystal Institute, Kent State University, Kent, Ohio 44242
(Received 26 December 1984; revised manuscript received 28 June 1985)

Computerized data-gathering techniques were employed to obtain electron-paramagnetic-resonance (EPR) probe molecule spectra reflecting the molecular dynamics of a typical nematic liquid crystal, MBBA, in the supercooled temperature region previously unaccessible to traditional analytical methods other than thermal analysis. Detailed line-shape simulations of the supercooled and glassy spectra recorded at 0° and 90° agree with the percolation model of glass formation, and confirm the validity of using extrapolated values of EPR and diffusion parameters from the nematic temperature region through the onset of the glass transition. Near this glass phase transition, from about 220 K and below, the spectra recorded at both 0° and 90° orientations are found to be the sums of liquid and rigid EPR spectra, providing further evidence for the coexistence of two different types of phase regions. Sudden changes in signal intensity observed at the glass transition are interpreted as resulting from EPR signal saturation effects associated with changes of T_1, the spin-lattice relaxation time, resulting from the change of a substantial amount of the sample from the supercooled liquid to the solidlike glass state. A faster molecular diffusion rate is observed at the glass transition for nematic liquid crystals than for isotropic liquids. This may be a result of the nematic order quenched into the glass.

I. INTRODUCTION

Liquid-crystalline glasses are unusual in that they combine the amorphous qualities of the glass state with the ordering of the liquid-crystal state.[1] Many different studies have probed some of the properties of this state through different experimental techniques, including amongst them differential thermal analysis (DTA),[1] different scanning calorimetry (DSC),[2,3] Mössbauer-effect studies,[4–6] Raman, ir, and far-infrared (FIR) spectroscopy,[3] diamagnetic susceptibility,[7] nuclear magnetic resonance (NMR),[8] and electron paramagnetic resonance (EPR) studies.[9,10] In addition to the determination of glass transition temperatures for both the main glass transition and liquid-crystalline chain-tail-melting transitions,[4,9] liquid-crystalline order parameters, Debye temperatures, and diffusion-related parameters are often computed.

In this study we use electron-paramagnetic-resonance techniques to extend our knowledge of the molecular dynamics of the liquid-crystalline nematic phase[11,12] into the supercooled liquid and glass regimes of the liquid-crystal glass. Along with some of the above-mentioned material parameters, anisotropic rotational-diffusion relaxation times, $\tau_{||}$ and $\tau_{\perp}$, are determined for the entire glass to isotropic temperature range and the EPR magnetic parameters are determined. Further, we could observe the liquid-crystalline glass in orientations both parallel and perpendicular to the liquid-crystal director axes, revealing important information about the molecular relaxation behavior at the glass transition and in the liquid-crystalline glass. A faster molecular diffusion rate is observed at the glass transition for nematics than for isotropic liquids. This information is viewed in light of the Grest-Cohen model of glass formation[13–15] and a two-dimensional model of the liquid-crystalline glass state.

The experimental methods used in this research are detailed in Sec. II of this paper and the above-mentioned results and discussion are found in Sec. III. Our summary and conclusions are presented in Sec. IV.

II. EXPERIMENTAL TECHNIQUE

Two nitroxide spin probes were dissolved into separate samples of MBBA, *n*-(*p*-methoxybenzlidene)-*p*-butylaniline, a nematic liquid crystal, and EPR spectra were observed from above room temperature to well below the reported main glass transition temperature of $T_g = 201–206$ K,[1,2,9,10] and also the reported chain-melting temperature of $T_{CM} = 176–193$ K.[4,9] MBBA has recorded transition temperatures as are shown in Fig. 1(a).[16] The literature values were confirmed with scanning thermal microscopy under crossed polarizers, to check that the presence of impurities and the EPR probe molecules was not great enough to change the clearing and melting-point temperatures.[17,18]

Two probes were used in these studies. A small nearly spherical, perdeuterated nitroxide spin probe, $C_6D_{16}NO_2$ (D-Tempone), 2,2,6,6-tetramethyl-4-oxopiperidinooxy was prepared at Kent State University. From its size and shape, one expects this probe to engage in nearly isotropic tumbling and to diffuse according to a free diffusion model. Tempone is mildly polar and therefore is expected to reside near the rigid polar part of MBBA, except at

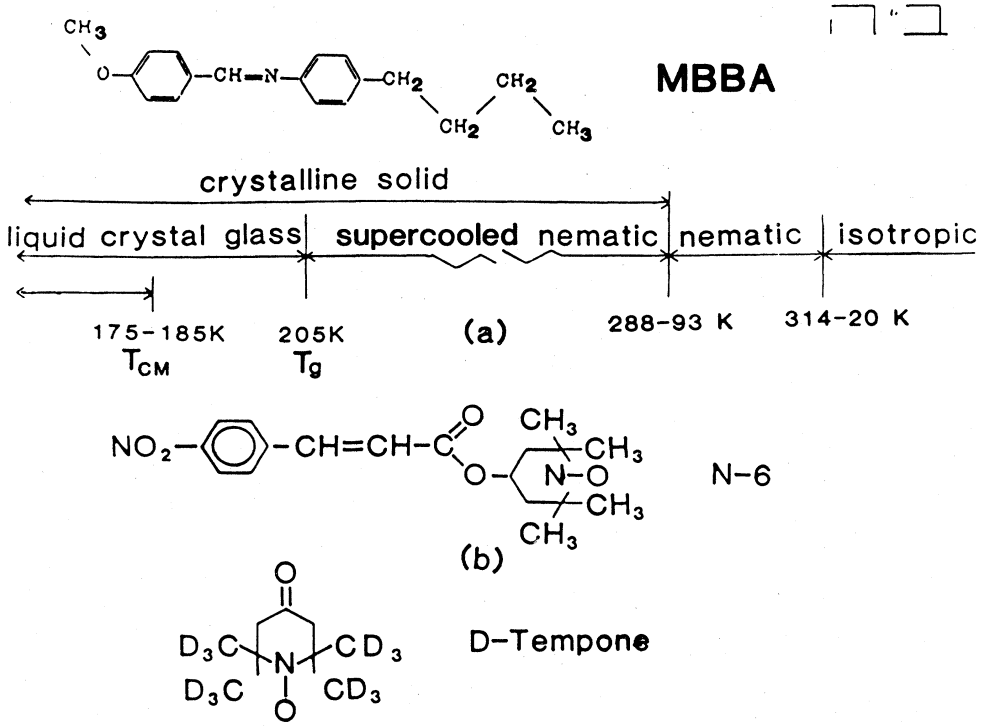

FIG. 1. MBBA structure and phase-transition temperatures are shown in (a). The main glass transition temperature is denoted as T_g, and the observed subsidiary chain-melting glass transition temperature is denoted as T_{CM}. (b) shows the chemical structure of the nitroxide probes N-6 and D-Tempone. The nitroxide N-O moiety is at the rightmost end of the N-6 probe.

lower temperatures when closer packing would force it out into the nonpolar chain region.[9] The probe was perdeuterated to minimize the inhomogeneous broadening observed before with the protonated probe, H-Tempone.[9] The other probe used was a long rodlike-shaped molecule, N-6, piperidinooxy-4-hydroxy-2,2,6,6-tetramethyl-*p*-nitrocinnamate, which was prepared by Sheley at Kent State University and discussed in Ref. 19. The chemical structure of both probes is shown in Fig. 1(b). The shape and size of N-6 leads one to believe that it will tumble anisotropically and undergo Brownian motion. EPR parameters for both probes are listed in Table I. These were obtained for N-6 from computer simulations based on starting values obtained from our previous study[9] and from the rigid-limit and fast-motion limit experimental spectra. The D-Tempone parameters were obtained from the experimental spectra, computer simulation of the fast-motion, isotropic spectra, and the literature.[18,20–23]

To obtain the glass state, each sample was alternately cooled and heated within the spectrometer cavity at rates estimated to be of between 10 and 30 K/min. Spectral measurements were recorded while continuously varying the temperature, at 10- to 20-K intervals, on numerous scans, sweeping both up and down from well below both glass transitions ($\approx$140 K) to within the liquid-crystalline nematic temperature range.[24] This procedure was made possible through the modifications made to the standard EPR setup described in the following.

The *X*-band paramagnetic resonance spectra were obtained using a modified Varian 4500 spectrometer. A Heath-Zenith H-89 microcomputer was interfaced with the spectrometer to record magnetic field and derivative absorption values, and to control the magnetic field. The computer interface allowed the magnet field to be swept through the 100-G sweep range in 8 sec. Generally, 6—14 spectra were recorded per temperature run, either sweep-

TABLE I. EPR magnetic parameters were obtained for the D-Tempone probe from the literature, and for the N-6 probe from best fits of simulated lines to observed spectra. For D-Tempone and N-6, $H_0=3330$ and 3323 G, respectively. For both probes, $\nu=9.27\times10^9$ GHz, $\omega_e=2\pi\nu$, and $\omega_n=(8.8\times10^6)a_n$. The D-Tempone probe has a T_2 of 0.29±0.05 G, whereas the N-6 probe has a measured T_2 of 1.00±0.25 G.

Spin probe	g_{xx}	g_{yy}	g_{zz}	A_{xx} (G)	A_{yy} (G)	A_{zz} (G)	a_n (G)
D-Tempone	2.0104	2.0074	2.0026	5.9	6.6	34.6	15.7
N-6	2.0542	2.0542	2.0446	6.47	6.47	34.1	15.7
	±0.0004		±0.0008				

ing up or down in temperature, and the spectra were saved on the data disks between temperature runs. The data obtained by our improved techniques were analyzed using hardware and software described elsewhere.[18,25]

A ramp generator was constructed for the Varian 4547 variable-temperature accessory. The time constant of the ramp circuit was varied to achieve the temperature sweep rates noted above. Even at the slow sweep rates crystallization of the MBBA sample was not found to be a problem. During the variable-temperature runs, the sample temperature was observed to vary from 5 to 20 K over the 8-sec sweep time of the spectrometer magnet B-field excursion. At temperatures above the MBBA melting point[16] of 20 °C, and temperatures below the main glass transition of $\approx$205 K, the sample temperature was held constant during the recording of spectra.[18,25]

The major experimental accomplishment of this work was the computer interfacing and programming enabling the recording of EPR spectra of the liquid-crystal sample in the supercooled region where longer sampling times would have included crystallization. This extends the availability of a molecular probe technique, dependent on the microscopic behavior of the material, to regions where previously only thermal scanning methods had access. The results of this extended investigation are reviewed and discussed in the next section.

III. RESULTS AND DISCUSSION

A. Temperature dependence of the spectra

The experimental results of our variable-temperature runs showing spectra of the D-Tempone and N-6 EPR probes are shown in Figs. 2 and 3, respectively. Additional "rigid-limit" spectra are shown in Figs. 7 and 8. These figures show rigid-limit spectra with the liquid-crystal director axis aligned both parallel (0°) and perpendicular (90°) to the laboratory magnetic field z axis.

The supercooled spectra do not vary considerably from what may be expected if one were to extrapolate EPR matching parameters from the rigid-limit and fast-motion regimes.

Spectra obtained with the liquid-crystal director rotated 90° perpendicular to the magnetic field were obtained below the glass transition temperature T_g. However, the MBBA was found to reorient and crystallize at temperatures 10—20 K above this temperature when the sample was allowed to sit for short lengths of time.[9,10] When the 90°-oriented sample was swept in temperature from the glass state to the supercooled-liquid state, the liquid-crystal director rapidly realigned with the spectrometer magnet B field. Spectra recorded in this temperature region show a composite spectrum of several molecular orientations between 90° and 0° superposed on one another.

B. Line simulation, S, τ, and Heisenberg spin exchange

Simulated "best-fit" matches[11,26,27] are also shown coincident with the N-6 spectra. Matches to D-Tempone spectra require the inclusion of diffusion parameters accounting for the slowly relaxing local structure (SRLS)

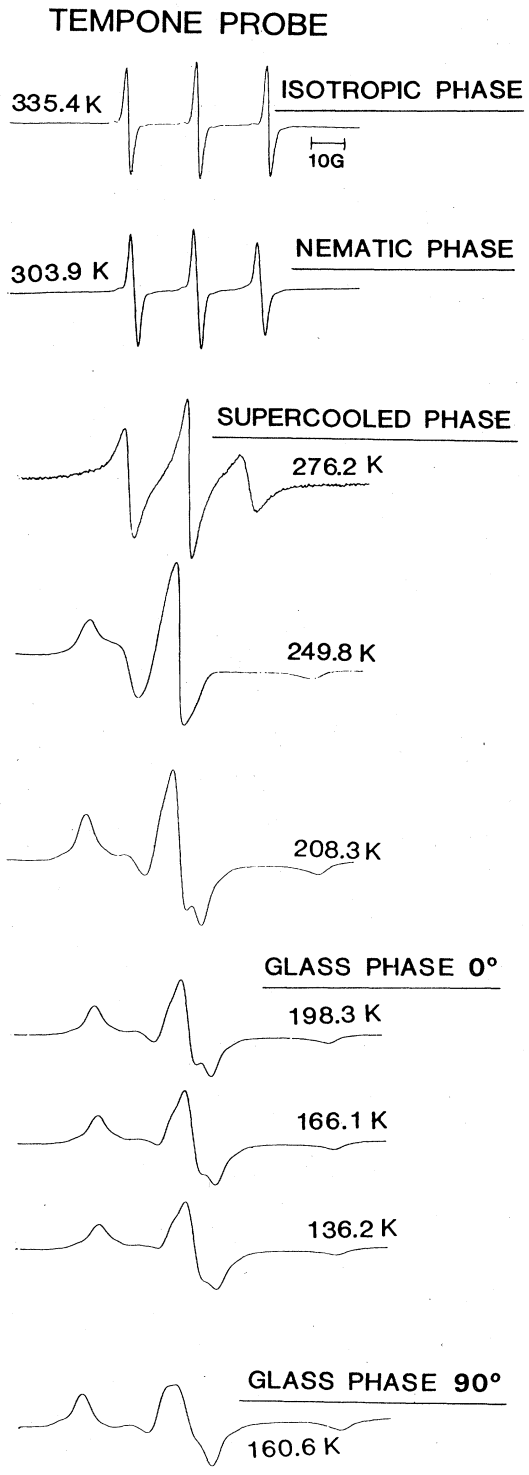

FIG. 2. Experimental EPR spectra from the MBBA isotropic phase, the nematic liquid-crystalline phase, the previously inaccessible supercooled nematic liquid-crystal phase, and the glass phase with the director oriented parallel (0°) and perpendicular (90°) to the magnetic B field are shown for the D-Tempone probe. Data from the supercooled region of MBBA were taken while the sample temperature was rapidly swept from glassy to nematic liquid-crystalline states.

that are found to be important in liquid-crystalline media.[12,23] Therefore, computer matches to the D-Tempone spectra were not made.

Spectral fits were made from visual comparison of the recorded experimental spectra and the computer-generated simulations, and also through minimizing a reduced χ value obtained from a comparison of 256 points of the two lines.

Other experiments have made extensive simulation studies of D-Tempone in MBBA and other liquid crystals at higher temperature,[23,28,29] and the interested reader may consult those works. Representative fits of the N-6 data, which exhibit Brownian motion,[30] are shown in Fig. 3.

Line simulations were made for the N-6 spectra and depend primarily on values of the material parameters: the anisotropic rotational-diffusion parameters τ, the Heisenberg spin exchange frequency ω_{SS}, the Saupe ordering parameter S, and the anisotropic magnetic parameters: the Landé g tensor, and the hyperfine A tensor. Starting values for the material parameters were obtained from the methods mentioned in the following paragraphs. Starting values for the magnetic parameters were obtained from the fast- and slow-motion limit spectra using standard EPR techniques.[25]

For the N-6 probe, $A_{||}$ is perpendicular to the long body axis of the molecule. We corrected for this so that the relaxation times, $\tau_{||}$ and $\tau_{\perp}$ here refer to the parallel and perpendicular diffusion of the probe molecule. In the fast-motion regime where the individual hyperfine lines are easily resolved, the starting values were often found to be within 15% of the simulated "best" fit. For the relatively large N-6 probe in the fast-motion region, inhomogeneous broadening can be expected to play only a minor role in the observed line shapes and need not be corrected for to obtain accurate results.[29,31] The N-6 probe molecule, not being deuterated, is expected, from the hydrogen hyperfine interaction, to exhibit more nearly Gaussian-shaped spectral lines, being narrower in the tail sections than Lorentzian spectral lines.[18] This was found to significantly affect our matches of the experimental, slow-tumbling 90°-oriented spectra.

The general spectral features of the simulation were found to be sensitive to even small changes in some parameters and insensitive to changes in other parameters.[18,26] The spectral features are sensitive to τ, S, and to ω_{SS}. In the intermediate-tumbling region, however, once $D_{xy}=1/(6\tau_{\perp})$, the diffusion coefficient about the molecular xy plane, was fixed, the line shape was somewhat insensitive to changes of $D_{zz}=1/(6\tau_{||})$, the diffusion constant about the molecular z axis. In the glass state, this parameter appears to be crucial as both 0°- and 90°-oriented spectra are readily observable. This phase of the material is further discussed below.

Starting values for the Saupe order parameter $S=D_0^2=\frac{1}{2}\langle(3\cos^2\theta-1)\rangle$ were obtained from isotropic and liquid-crystal $\langle a\rangle$ splittings, the EPR probe magnetic tensor values, and the relation[32]

$$S=\frac{\langle a\rangle-a_N}{2(a_N-A_{\perp})}, \tag{1}$$

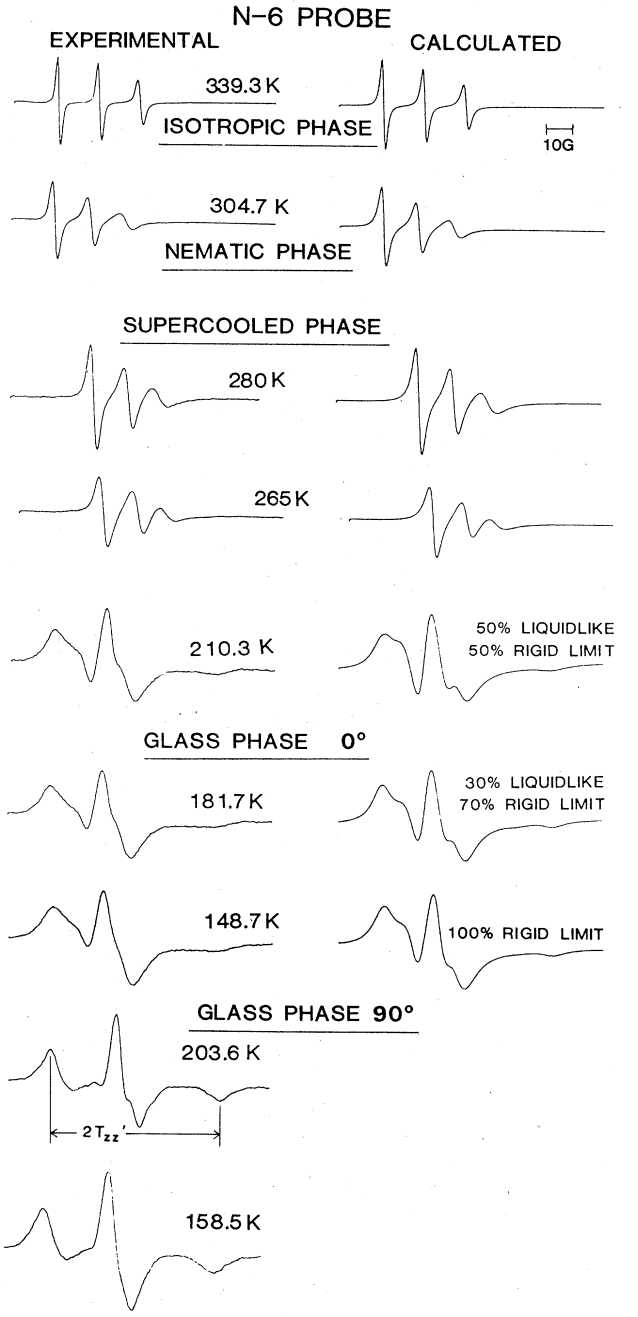

FIG. 3. Experimental and calculated computer-matched EPR spectra from the MBBA isotropic phase, the nematic liquid-crystalline phase, the previously inaccessible supercooled nematic liquid-crystal phase, and the glass phase with the director oriented parallel (0°) and perpendicular (90°) to the magnetic B field are shown for the N-6 probe. Data from the supercooled region of MBBA were taken while the sample temperature was rapidly swept from glassy to nematic liquid-crystalline states. EPR parameters used for the matches are shown in Figs. 4–6 and Table I. Glassy and near-glass fitted spectra are composed of varying percentages of rigid-limit and fast-tumbling spectra, with the matches at 210.3, 181.7, and 148.7 K being, respectively, 50%, 70%, and 100% rigid-limit spectrum. The rigid-limit spectrum has $\tau_{\perp}=1.7\times10^{-7}$, $\tau_{||}=1.1\times10^{-8}$, $S=0.165$, and $\omega_{SS}=20$ MHz.

where $\langle a \rangle$ is the experimental splitting between the individual spectral lines, a_N is the average splitting of the fast-motion limit, isotropic spectrum, and $A_\perp$ is the average perpendicular component of the hyperfine A tensor. For the slow-motion tumbling regions, the lowest-temperature liquid-crystalline spectrum was used for a starting S value. The values from this relation represent the order of the nitroxide moiety. They may be scaled times -2 to show ordering about the liquid-crystal director. A plot of S versus T is shown in Fig. 4 from the N-6 spectra. Values are plotted from Eq. (1) and from our simulations to the experimental data. For the 0° spectra, one finds that the Saupe order parameter S remains mostly constant in the supercooled liquid crystal temperature range.

Rotational correlation times τ were calculated for all the spectra gathered in several ways. For the purposes of calculating τ, it is convenient to view the EPR data as divided into two tumbling groups, fast and slow. The data of the fast-tumbling isotropic region is adequately described by motional narrowing theory,[9,28,31,33] from which it is easy to calculate perpendicular, parallel, and average rotational correlations times, τ. In the ordered, liquid-crystal, phases of the sample, these methods are inadequate,[12] as the fast-tumbling formulas will give nonphysical results if applied without caution. However, the value calculated for $\tau_\perp$ using these methods does give the approximate correct value for τ, even in the ordered regimes.[11,12,28]

A plot of $\log_{10}\tau$ versus $1/T$ is shown for the values calculated from the fast-motion theory and line simulations for N-6 in Fig. 5(a). A similar plot for D-Tempone is shown in Fig. 5(b) using values obtained from the fast-motion theory. One finds that the molecular diffusion times τ, fall on a curve extrapolated from the liquid-crystalline liquid to the glassy, slow-tumbling region.

This data is matched with the Stokes-Einstein relation for τ, $\tau = 4\pi a^3\eta/3kT = A_0\eta/T$, where a is related to the molecular radius, kT is the thermal energy, and η is the viscosity. In the liquid-crystalline regions, the τ relaxation data is fit with the Grest-Cohen percolation model for η.[13] Here, the liquid-state viscosity is found as a function of a molecular free volume, dependent on temperature and the formation of liquidlike and solidlike clusters in the near-glass and glassy material. The viscosity is found from a free-energy calculation, and depends on the glass transition temperature T_g, with a finite free volume even at temperatures well below the glass transition. One may find τ as

$$\tau_1 = \frac{\tau_{01}}{T}\exp\left[-\gamma\frac{v_0}{(T-T_g)+[(T+T_g)^2+\beta T]^{1/2}}\right]. \quad (2)$$

The fitting parameters for these matches are shown in Table II. For the N-6 data, the local microviscosity, η was also calculated according to our extension[18] of the Grest-Cohen model so as to be valid for the regions both above and below the glass transition temperature,

$$\tau^{-1} = (\tau_1)^{-1} + (\tau_2)^{-1}, \quad (3)$$

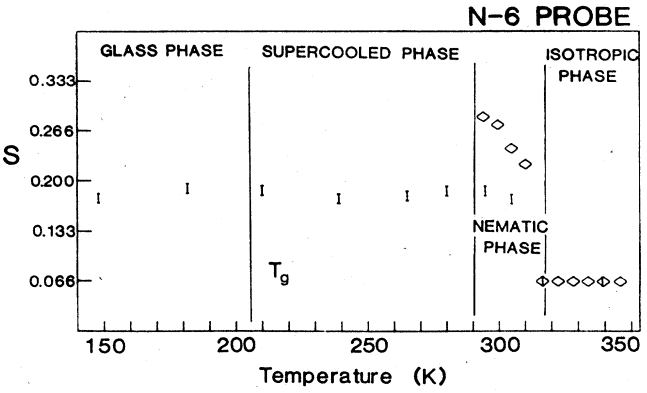

FIG. 4. Liquid-crystalline order parameter S plotted vs temperature T for the N-6 probe. Order parameters for the N-6 probe from our computer simulations (I) and from Eq. (1) (◇) are shown.

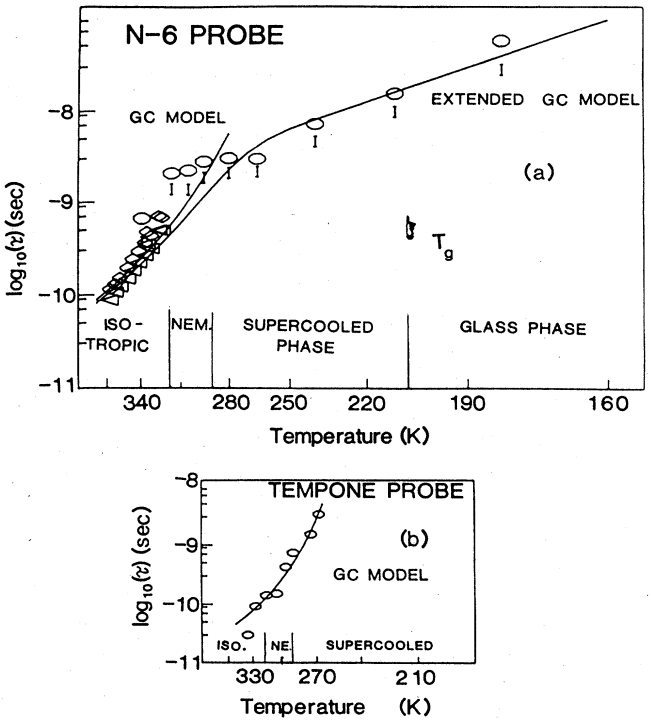

FIG. 5. $\log_{10}\tau$ vs $1/T$ is shown for the values calculated from the fast-motion theory and line simulations for N-6 in (a). Value calculated from the fast-motion model are ◁ for $\tau_{||}$ and ◇ for $\tau_\perp$, while those values found from computer matches are I for $\tau_{||}$ and ○ for $\tau_\perp$. The two fits shown are (1) from the Grest-Cohen model for viscosity η in the high-temperature region and (2) from our extension of this model for microviscosity, valid even in the glass state. A similar plot for D-Tempone is shown in (b) using values obtained from the fast-motion theory. The values are those found for $\tau_\perp$. Line fit is from the Grest-Cohen viscosity model. Fitting parameters for the curves of these figures are found in Table II.

TABLE II. Activation rates and energies for N-6 in MBBA, in the liquid (l) and glassy (g) states, are calculated assuming Arrhenius behavior. Glassy-state values from our fit to Eq. (3) are also shown. Values for the D-Tempone fast-motion region are also recorded. Lower part of the table shows the matching parameters from Eq. (2), the Grest-Cohen viscosity model fitted with the Stokes-Einstein relation for both probes in the high-temperature, liquid state.

Probe	$A_l\eta$ (sec)	$\Delta E/R$ (K)	$A_g\eta$ (sec)	$\Delta E/R$ (K)
N-6	1.13×10^{-13}	4639	1.32×10^{-8}	1121
N-6 (fitted)			3.23×10^{-8}	979
D-Tempone	1.19×10^{-15}	5436		

Probe	τ_{01} (sec)	γV_0 (K)	T_g (K)	β
N-6	1.52×10^{-9}	1104	204	4.03
D-Tempone	1.14×10^{-9}	715	214.7	0.307

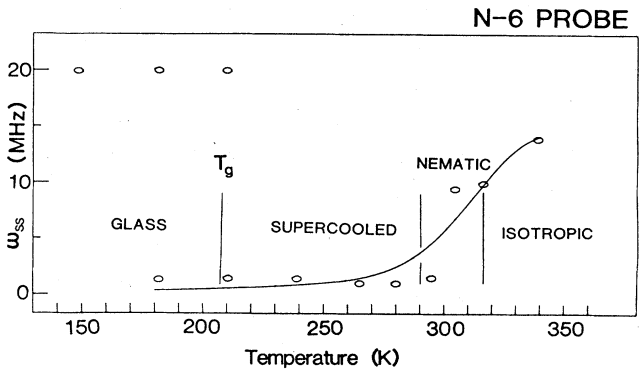

FIG. 6. Plotted here is ω_{SS} vs T for N-6. The curve is a least-squares fit to the data of Eq. (4), with N-6 parameters of $A'=4.7\times10^{-9}$, $B'=1.1$, $C'=1.5\times10^{-3}$, and $D'=-0.21$. For temperatures below $\approx$220 K, ω_{SS} values are shown for both the slow-motion tumbling and rigid-limit component spectra of the composite simulated spectra.

where

$$\tau_2=\frac{\tau_{02}}{T}\exp(\Delta E/RT)\ .$$

Here, τ_2 is the local microviscosity of the liquidlike "pockets" of the glass region, τ_{02} is an activation rate for the liquidlike portions of the glass region, ΔE is an activation energy for diffusion in this region, and R is the universal gas constant.[18] Equation (3) is matched to the data in Fig. 5(a). Additional liquid-state activation-energy values for both probes and glassy values for N-6 are listed in Table II.

Another of the fitting parameters found to be critical for accurate line-shape simulation in the slow-tumbling regime of the EPR Lanczos algorithm program[26,27] is the Heisenberg spin exchange frequency, ω_{SS}.[18,25,34,35,38] This interaction is a result of bimolecular collisions of radicals when an exchange integral J' is present. One finds that an additional term must be added to the spin Hamiltonian, H_{SS}, that is dependent on time because of the relative motion of the radical pairs. The apparent effect is to cause an exchange of nuclear environment for the electron spins. The effective exchange frequency ω_{SS} from the rotational-diffusion value using the relation for τ for Eq. (3) is[18]

$$\omega_{SS}=\frac{B'\tau/A'}{(\tau/A')^2+C'}-D'\ , \tag{4}$$

where A', B', C', and D' are fitted constants. We found that even at short rotational relaxation times, a residual ω_{SS} should be included to best fit the experimental data, therefore necessitating the additional D' constant. One may match the ω_{SS} values used in the line simulations to this equation, as has been done in Fig. 6. The shape of the curve and the corresponding matches are considered with strong exchange, $J\tau\gg1$ ($J=2J'$), at higher temperatures. This relationship changes in the glass state, where a larger ω_{SS} value is observed for the rigid-limit spectrum.

C. Ordered glassy spectral matches; slow-tumbling plus rigid-limit nematic spectra

At temperatures well above the glass transition the probe may be thought to undergo nearly uniform relaxation. The observed spectra can be well fit with a single spectrum characterized by a single rotational-diffusion time and a fixed parallel-to-perpendicular tumbling ratio. At lower temperatures, the spectra were found to be best fit with a linear combination of a slow-tumbling (large-τ) spectrum and rigid-limit (τ maximum) spectrum. The lowest-temperature spectrum that we observed for each probe, 148.7 K for N-6 and 136.2 K for D-Tempone, is taken as the rigid-limit spectrum. The rotational-diffusion time used for the liquidlike component of each match is based on starting values extrapolated from the phenomenological models previously described.[18] At temperatures below the glass transition, the observed spectra are best fit with 50—100 % rigid-limit spectrum (depending on temperature) and the balance slow-tumbling spectrum. In this temperature region the dominant spectral shape is that of the rigid-limit spectrum. The general spectral shape would appear to be independent of temperature, but many of the spectral details are influenced by the slow-tumbling spectrum that is still part of the composite spectrum. As the temperature is raised above the glass transition, the observed spectra are best matched using smaller percentages of the rigid-limit spectrum, with the relative percentages of liquidlike and solidlike spectra following a step function at the glass transition temperature (see Fig. 3, the graph of p, the percentage of liquidlike cells from Ref. 18). Since the observed spectra appear to be sums of slow-tumbling and rigid, solidlike spectra, these observations provide support for the Grest and Cohen percolation model of the glass.

From the glassy- and liquid-state activation-energy values of Table II it is possible to estimate the percentage of liquidlike cells at the onset of the glassy state, p_c.[18] For p greater than the critical concentration p_c, there exists an infinite, connected liquidlike cluster. One may

consider the material within this infinite cluster to be a liquid.[13] We find p_c equal to 0.24 ± 0.03 for N-6 in MBBA. Our experimental "difference" spectra discussed below suggest a p_c value of ≈ 0.30 for the main glass transition for both probe molecules. Also, the simulated N-6 spectrum just above T_g at 210.3 K shows a 0.50 liquidlike component. Both of these results agree well with that calculated from the activation energies and the percolation model. The product $a_z(p)A_z(p)$ of the percentage of liquidlike cells that belong to liquid clusters, $a_z(p)$, and the number, $A_z(p)$, of clusters larger than some minimum value v_m, is found in the glassy state from the activation rates and p_c to be equal to $(3.5^{+6.6}_{-2.3}\times 10^{-15})$.[18] This result suggest that the liquidlike clusters of the nematic glass are few and small in size.

This model implies that the primary objective in fitting glassy spectra is in finding a rigid-limit simulation that closely matches the observed experimental rigid-limit spectrum. Thus, the 0°-oriented matches from Fig. 3 are predominantly composed of the rigid-limit low-temperature spectra there displayed. We were unable to find a good match to the 90°-oriented rigid-limit spectrum of N-6, even though this spectrum should be obtainable simply through introducing a 90° rotation into the simulation program. Some reasons for this failure are worth examining. One reason already discussed is inhomogeneous line broadening from the hydrogen hyperfine interaction of the nondeuterated probe. A similar problem was found in another work when trying to match spectra from the H-Tempone probe in an isotropic liquid prompting a change to deuterated Tempone in later work.[18] Another possible reason for the difficulties encountered in matching the perpendicularly oriented glassy spectra may be found in the glass state itself. One might expect that the solidlike components of the glass can align themselves perpendicular to the EPR magnet B field when the sample is rotated, but there is no inherent reason the liquidlike components should do likewise. One expects that, to the extent of their freedom of motion and ability, the liquidlike components of the glass would reorient themselves with the magnetic field in a direction perpendicular to the solidlike components. This would also change the simple single-line spectra. Further experimentation may be useful to test these hypotheses and suggest others.

When simulating the N-6 spectra recorded above the glass transition temperature, one finds a ratio of about 1.5:1 between the parallel and perpendicular molecular diffusion constants gives a good fit to the experimental data. Previous studies of a similar nitroxide spin probe in liquid-crystal media in nematic and smectic phases of higher order exhibited values for N, the anisotropy ratio of the diffusion tensor, of from 3 to 20.[11] As mentioned earlier, our spectra were largely insensitive to this parameter.

From the Grest-Cohen percolation model of the glass state one expects to find liquidlike clusters amongst the solidlike sites of the nematic glass. These liquidlike clusters may be thought of as having properties similar to those of the supercooled nematic liquid crystal. Clusters of liquidlike cells might form ovoid-shaped pockets amidst the solidlike cells. These pockets may be viewed in a polar coordinate system as a two-dimensional (2D) glass[37–39] with free diffusion in the θ direction and restricted diffusion in the ϕ and r directions.

As is characteristic of 2D solids, one may find an order parameter for the nematic glass, namely the Saupe ordering parameter S. This is the nematic short-range orientational order "quenched" into the glass state. The presence of the magnetic field while the sample is quenched would tend to align the nematic monodomains and give a long-range orientational order through the whole sample.

The existence of liquidlike percolation clusters appearing as defects[40] would increase the breakup of glassy long-range positional order. Normally,[38,39] no long-range positional order may be expected to exist.

The nematic glassy percolation phenomena[14,15] may be compared to the melting of classical 2D solids.[37,38] The primary mechanism for percolation is the growth of liquidlike clusters. This growth may proceed through the formation of edge disclinations or screw dislocations at the boundaries of the existing liquidlike clusters. As in 2D solids where disclination pairs are thought to be found first at the edges of the 2D solid, in the 2D solid plane, here, too, disclination or screw dislocations could be seen as a growth from a liquidlike cluster into the r or ϕ directions, which are normally solidlike. The result could be a growth of the glassy nematic cage or cluster, as is also found with an isotropic glass. This would lead eventually to the formation of an infinite connected liquidlike cluster at T_p, the percolation temperature. This result is more pronounced in the ordered liquid-crystal glass than in the isotropic glass. It may be the cause of glass formation at faster relaxation times than was observed in isotropic liquids.[18,41]

Another simple experimental demonstration supporting the two-tumbling-site model can be graphically given by comparing the recorded spectra immediately above and below the nominal glass transition.[18] According to our model the spectrum just above the glass transition should reflect primarily liquidlike cells, whereas the spectrum just below the glass transition should reflect a primarily solidlike material. Subtraction of a small percentage of the liquidlike spectrum above T_g from the mostly solidlike spectrum below T_g should leave one with a spectrum reflecting almost only solidlike tumbling centers. This difference spectrum can be compared to a rigid-limit spectrum, or else to the lowest-temperature spectrum experimentally recorded that may be used as an approximation to this theoretical limit. This can be done for both the 0° and 90° spectra for both spin probes studied. Figure 7 is our attempt at this procedure for the N-6 data and Fig. 8 our results from the D-Tempone spectra. We will discuss the N-6 probe results first here because its analysis is simpler. For N-6, the two 0° spectra plotted are (1) the different spectrum [highest-temperature glass spectrum (198.9 K) minus 30% of the lowest-temperature liquid spectrum (210.3 K)] and (2) our lowest-temperature rigid-limit spectrum at 148.7 K. The match is seen to be reasonable. The 90° liquidlike spectrum is found to be physically nonexistent as the sample realigns parallel to the magnetic field as it warms up out of the glass state, before recrystallizing. Even in the fast temperature sweep

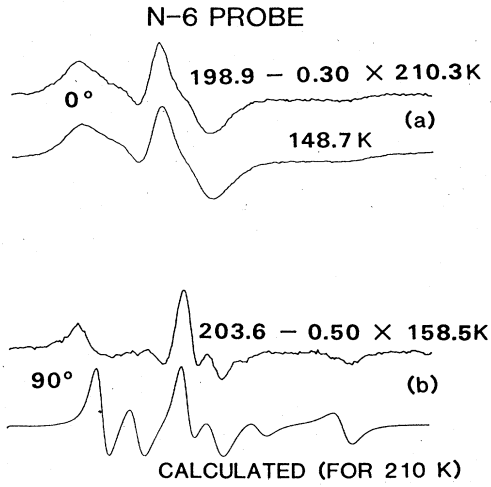

FIG. 7. (a) For N-6, the two 0° spectra plotted are (1) the difference spectrum [highest-temperature glass spectrum (198.9 K) minus 30% of the lowest-temperature liquid spectrum (210.3 K)] and (2) our lowest-temperature rigid-limit spectra, at 148.7 K. (b) The 90° liquidlike spectrum is found to be physically nonexistent as the perpendicularly oriented sample realigns parallel to the magnetic field as it warms up out of the glass state, before recrystallizing. Here, it is constructed as the difference of the 90°-oriented high-temperature glass and the rigid-limit spectra. This is compared with a simulated 90°-oriented spectrum with $\tau_{\perp}=1.85\times10^{-8}$, $\tau_{\parallel}=1.11\times10^{-8}$, $S=0.165$, and $\omega_{SS}=1.4$ MHz.

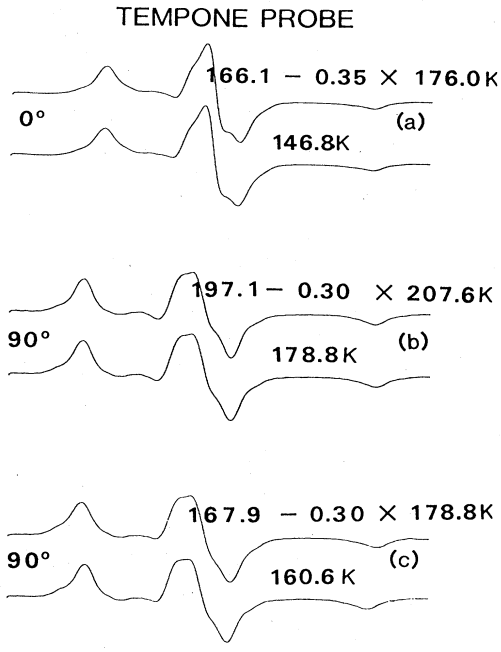

FIG. 8. The D-Tempone 0°-oriented difference spectrum, around the chain-melting transition of $\approx$170 K, and the 0° rigid-limit spectrum are shown in (a). The difference spectrum around the main glass transition (205 K) and the rigid-limit spectrum are shown in (b), for the 90° sample orientation. (c) shows the difference spectrum and the rigid-limit spectrum of the chain-melting transition from the perspective of the 90° orientation.

mode, the sample spectra were observed not to maintain an orientation perpendicular to the magnetic field in the supercooled liquid long enough to observe a 90° liquidlike spectrum. However, one may still compute what this spectrum may look like from the experimental data as the difference of the perpendicular glassy spectrum just below the glass transition temperature minus a large part of the rigid-limit perpendicular glassy spectrum. This imaginary perpendicular supercooled-liquid spectrum may be compared with a simulated spectrum with the same estimated physical parameters. This is done for the N-6 perpendicular orientation in Fig. 7 with moderate success. The spectrum matched is the high-temperature glass (203.6 K) minus 50% of the rigid-limit (158.5-K) 90° spectrum. Some of the features of the "perpendicular liquidlike" spectrum are matched as the 90° orientation of the corresponding 0° 210-K liquidlike theoretical-experimental match.

Fitting the D-Tempone probe is more complicated because of its small size. We expect that, at low temperatures, the D-Tempone probe would lodge in the tail regions of the MBBA molecule and would detect the chain-melting glass transition,[4,9,42] instead of the main glass transition as has been previously reported. This chain-melting transition in MBBA has been reported at 175—185 K from Mössbauer studies[4] and around 190—193 K in an earlier EPR study using the nondeuterated H-Tempone probe.[9] In this work, one would therefore expect the spectral line-shape changes revealing the glass transition to occur about this same temperature range. Observation of spectral lines at 0° and 90° orientations surprisingly show both the main glass transition and the chain-melting transition. The transition from the unchanging rigid-limit glassy powder pattern to a changing, almost rigid-limit spectrum occurs in both the 0° and 90° orientations at between about 167 and 180 K, as may be seen from Figs. 2 and 8. This change is more pronounced in the perpendicular orientation than in the parallel orientation. The perpendicular (90°) orientation shows another spectral line change above the main glass transition temperature around 210 K. One may still observe 90° spectra of the D-Tempone probe well above the observed chain-melting temperature up to roughly the same temperature where the N-6 probe was seen to reorient and crystallize. Thus, as one sweeps through the main glass transition temperature, one may observe another change in the 90° D-Tempone spectra, corresponding to increased molecular diffusion and narrower spectral lines at the nominal T_g (see Fig. 2). Even though simulations were not done on these D-Tempone spectra, the "difference-spectrum" technique used with N-6 should also be applicable to both of the transitions observed with D-Tempone. For the 0°-oriented spectrum, at the chain-melting transition, $\approx$170 K, Fig. 8(a) shows the difference spectrum (166.1-K spectrum minus 35% of the 176.0-K spectrum) and the rigid-limit spectrum at 146.8 K. Around the main glass transi-

tion (205 K), Fig. 8(b) shows the 90°-oriented difference spectrum (197.1-K spectrum minus 30% of the 207.6-K spectrum) and the rigid-limit (178.8-K) spectrum. Here, the rigid limit is taken as just above the chain-melting temperature. For the 90° orientation the chain-melting transition is shown with the difference (167.9-K spectrum minus 30% of the 178.8-K spectrum) and rigid-limit (160.6-K) spectra [Fig. 8(c)]. The 0° D-Tempone spectra near the main MBBA glass transition temperature do not show major line-shape changes. However, as will be discussed later, saturation phenomena are considered as the cause of a change in line height and intensity also seen at this transition.

Thus, we are able to show glassy spectra as being comprised of parts of more elemental liquidlike and solidlike spectra. Although this model is a simplification and necessarily neglects the interactions between the component parts of the system, it seems to adequately meet the test of practical utility in matching the experimental spectra and is theoretically plausible.

In our earlier work on an isotropic glass,[18] it was found below temperatures of 30—40 K above the glass transition, that the hyperfine A-tensor appeared to increase. Although these spectra may have been fit through an increase in the average hyperfine-splitting tensor of about 1 G, we chose instead to fit them with a linear combination of liquidlike and solidlike rigid-limit spectra, with the percentage of liquidlike and solidlike spectra following a percolation model, as is discussed above. Alternate explanations of the apparent hyperfine A-tensor increase could include those of Meirovitch *et al.*[11] and Lee and Ames,[43] who observed hyperfine tensor changes caused from distortions of the piperidine ring and temperature effects, respectively. In this work, these explanations are ruled out through a careful examination of the parallel and perpendicular glassy N-6 spectra. For the 0° orientation, no increase in the average hyperfine A-tensor value is required to match the EPR spectra from the isotropic liquid phase through the liquid-crystal phases, the supercooled-liquid state, and the glass state, whereas greatly decreased molecular diffusion constants are still required to fit the glassy spectra. The apparent increase observed in the hyperfine A-tensor of the previous work in an isotropic media does not occur. The perpendicular (90°) spectra try the model, as these spectra show a much larger $2T'_{zz}$ (see Fig. 3, 90° spectra). One would expect that it is necessary to only include a 90° rotation of the liquid-crystal director tilt axis into the simulation program to match the perpendicular orientation of the same-temperature 0° experimental spectrum. Even though the 0° spectrum may be fit well with intermediate- to slow-tumbling time diffusion constants, rotating the director by 90° gives a simulated spectrum with an apparent hyperfine A-tensor splitting much too small to match the experimental 90° $2T_{zz}$ splitting. Only through greatly increased diffusion times is this computer-simulation splitting value brought in line with that experimentally observed. As before, the increased splitting could be matched with an increase in the A-tensor, however, this is theoretically unreasonable as the parallel-orientation spectra would no longer match.

Therefore, our data gives support in favor of fitting the observed spectra in the thermal region from 230 K to well below the glass temperature with linear combinations of rigid-limit and slow-tumbling spectra, and we feel that this result gives evidence favoring current glass theories.

D. Transition line shapes, line heights, spectral transforms, and line intensities

Although the measured liquidlike τ rotational correlation time undergoes no sudden changes at T_g with the N-6 probe and at T_{CM} (the chain-melting temperature) and T_g with the D-Tempone probe, there are several readily observable spectral line features that undergo pronounced changes at the glass transition temperatures in both 0° and 90° spectra. These may be accounted for from the expected "solidification" of the $(1-p)$ solidlike cells at the glass transition temperature, and from subsidiary effects. The spectral line shape takes on a mostly unchanging powder-pattern form at T_g,[9,41] which is maintained except for small changes at all recorded lower temperatures. This can be seen easily (Figs. 2, 3, 7, and 8) from plots of the lowest-temperature spectra scaled to all have the same height. At the same time that the spectral shape assumes a mostly unchanging form, one finds a distinct transition marker in the spectrometer signal intensity levels and in the spectral line heights.[9,41] Figure 9(a) shows a plot of integrated intensity for the 0°-oriented N-6 and D-Tempone data, and Figs. 9(b) and 9(c) are the corresponding plots for the 90°-oriented spectra. Figures 10(a) and 10(b) are plots of the relative height of the central spectral line of the 0°- and 90°-oriented N-6 data. Figures 10(c) and 10(d) are the corresponding plots for the D-Tempone probe.[18,44] The integrated values were obtained from the derivative spectra using an assembly-language program that iteratively solves for the proper zero baseline.

One may apply the same power "saturation" reasoning to these results as was used in the isotropic glasses previously studied.[18,44] There we found the spectrometer signal intensity to be proportional to I,[18,45]

$$I(T)=n/T+b=\frac{n^0/T}{1+2PT_1}+b\ , \tag{5}$$

where $n=n_l-n_u$ is the difference in population of the lower and upper energy levels, n^0 is the thermal equilibrium population difference, P is the stimulated emission coefficient, and b accounts for the background. This saturation equation exhibits a $1/T$ Curie-law dependence in the high temperature, fast-motion range, yet saturates at lower temperature as the spin-lattice relaxation time T_1 increases with increasing molecular diffusion times τ. The spin-lattice relaxation time in liquids is found as[18,44]

$$\frac{1}{T_1}=\frac{2g^2\beta^2}{h^2}\langle\,|H(t)^2|\,\rangle\frac{\tau}{1+\epsilon\omega_0^2\tau^2}\ , \tag{6}$$

where g is the Landé g factor, ω_0 is the spectrometer frequency, and ϵ is a fitted factor to account for shifts from Brownian motion of the spin probe,[29] which is expected to be about 1 for N-6 and 5 for D-Tempone. The solid curve drawn fitted to the data of Fig. 9 is a least-squares fit to the Curie law, Eq. (5), with the liquid-state relation for

T_1, Eq. (6), and the all-temperature rotational-diffusion relation, Eq. (3), used to calculate the rotational-diffusion correlation time τ. The final form of the fitting equation in this simple model is

$$I(T)=\frac{B_1/T}{(1+PT_1)}+B_3\ , \tag{7}$$

where

$$PT_1=B_2\frac{(1+\epsilon\omega^2\tau^2)}{\tau}\ ,$$

with B_1, B_2, and ϵ as fitting constants with easily determinable physical meaning, and an additional y-axis shift value B_3 required to match the experimental results. The fitting parameters for Eq. (3) found from the match to Fig. 5(a) were substituted into this fit without further modification. With the observed scatter in the data the fit

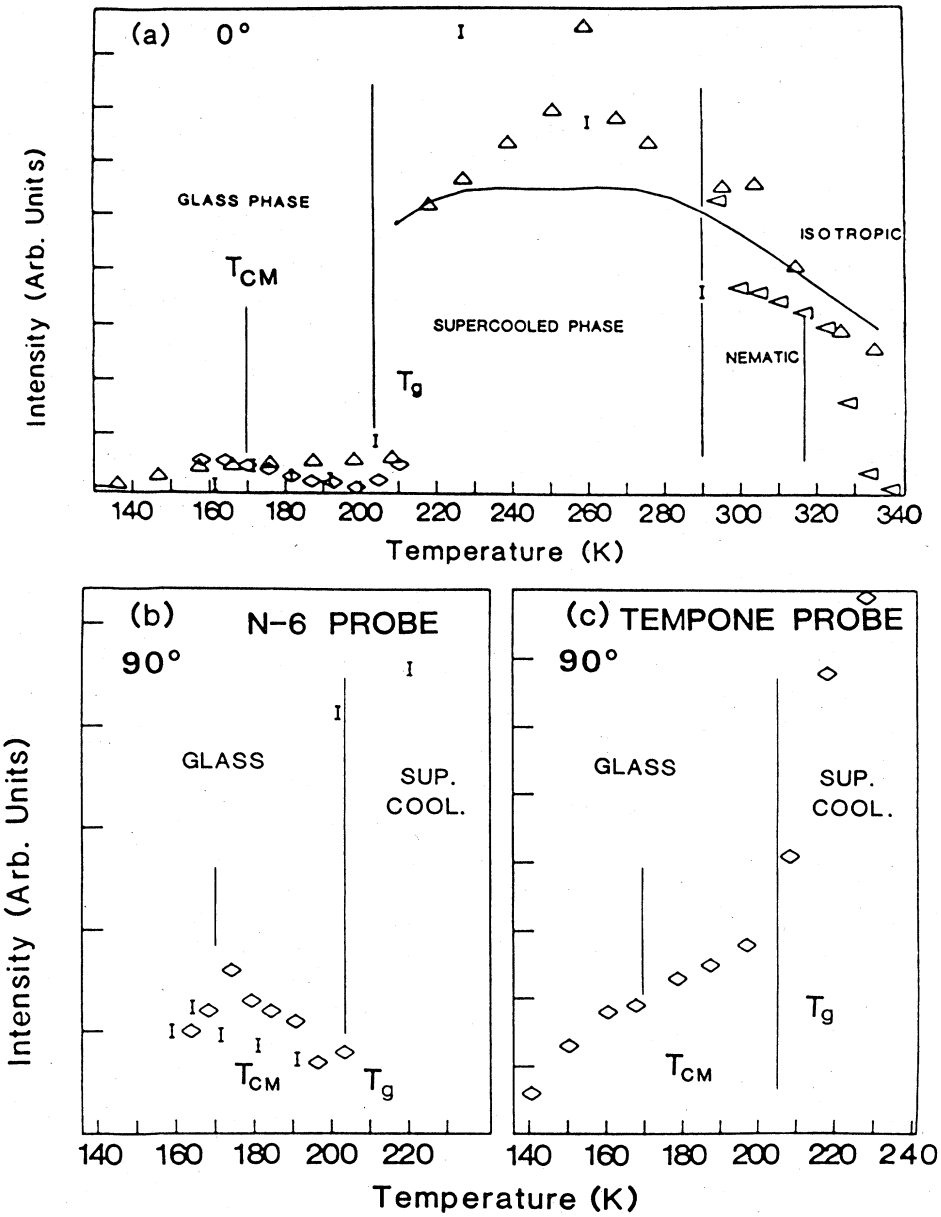

FIG. 9. The measured integrated intensity is plotted as a function of temperature here for (a) parallel, and (b) and (c) perpendicular, orientations of the aligned liquid-crystal samples. The N-6 (◁,I,◇) and D-Tempone (△) 0°-oriented data are plotted together in (a). The different markers for each probe correspond to separate runs of data. Plotted curve is a fit of the N-6 data only to Eq. (7) and our all-temperature microviscosity τ formula, Eq. (3), of Fig. 5(a). The fitting program used minimizes the maximum absolute error of the curve from the data. Fitting parameters used are $B_1=2653$, $B_2=1.9\times10^{-15}$, $B_3=-3.6$, and $\epsilon=4.8$. (b) shows the integrated intensity data of the 90° orientation of the N-6 MBBA sample and (c) the corresponding plot of the D-Tempone probe data. The effects of the main glass and chain-melting transitions are clearly seen near where these transitions are marked.

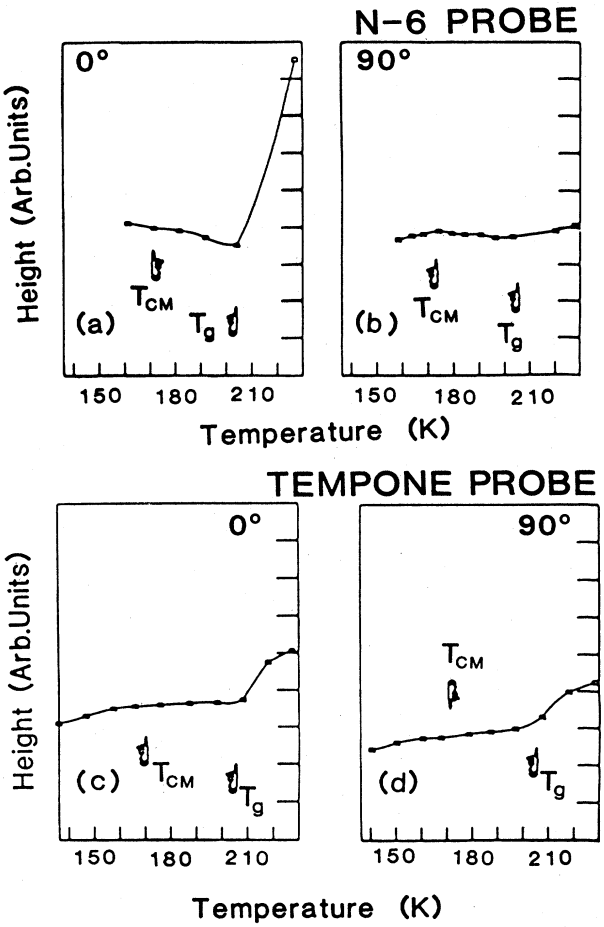

FIG. 10. Relative heights of the derivative spectral central line are plotted as a function of temperature. 0° orientation of the N-6 sample is shown in (a), and the 90° orientation in (b). Corresponding D-Tempone results are plotted in (c) and (d). Relative minima in the cubic-spline line fits are listed in the text.

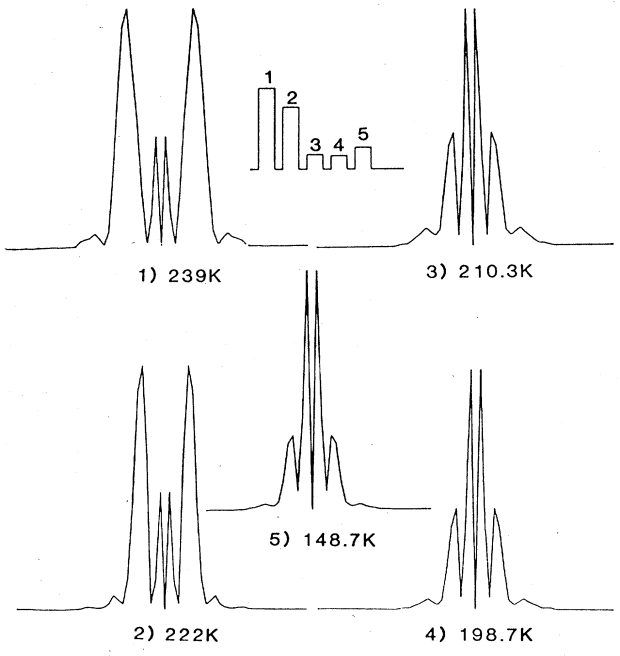

FIG. 11. Autocorrelation functions of some N-6 and MBBA low-temperature spectra are plotted to the same scale. Higher-frequency component lines are seen to largely vanish below the main glass-transition temperature. Here, 1 and 2 show above-T_g spectra, while 3 and 4 are just around the transition and 5 is the rigid-limit spectrum. Inset shows the relative scaling factor of each spectrum. The glass transition appears both in the frequency distribution of the power-density spectrum, and the overall power absorbed, as may be seen from the inset.

does not appear to be overly sensitive to the value of ϵ.

Within the glass state, one may expect this relation for simple fluids not to hold for T_1. One may expect a decrease in the spin-lattice relaxation time resulting from an increasing number of phonon relaxation modes in the solid state, and a consequent increase in spectrometer signal intensity. This would then account for the observed reversal or deceleration of the decrease in line heights and signal intensity noted at the glass transition and chain-melting temperatures as resulting from saturation effects.

The D-Tempone probe exhibits in our current work only a leveling of the peak-height decline without further increase at the chain-melting transition temperature (165—175 K). The D-Tempone probe in MBBA also records the main glass transition temperature T_g as another leveling of (1) intensity decline (Fig. 9) and (2) transition line height, with a 0°-oriented minimum of 208 K, as is apparent from Fig. 10. These effects are observed both in the 0° and 90° spectra. For the N-6 probe, the central line height and signal intensity decrease from a high value, some 30—40 K above T_g. The decline is reversed just below T_g. One finds the glass transition in a line height and intensity valley, and one may compute an experimental T_g from the minimum of fitted cubic splines to these figures (Figs. 9 and 10). For the N-6, 0°-oriented probe, a line-height minimum at 206.4 K is found. The 90°-oriented probe has local line-height minima of 201.6 and 187.0 K. These may be viewed as marking the main and chain-melting glass transitions. This effect was also seen with nondeuterated H-Tempone, as well as N-6 in earlier studies.[9,18,41]

In an attempt to better examine the underlying phenomena behind these line-shape changes, we took power-spectrum analyses (autocorrelation functions) of all our near-glass and glassy spectra.[18,46–50] One may use the spectral density function as a window to view the underlying frequency, and hence, linewidth distribution of in particular the intermediate- and slow-tumbling spectra. Peaks closer to the edges of the spectra of Figs. 11 and 12 represent higher-frequency components in the EPR spectra, thus reflecting narrower absorption or derivative lines, and are predominant in fast-motional high-temperature spectra. Peaks closer to the center of spectra from Figs. 11 and 12 represent low-frequency components of the EPR spectra, reflecting wider lines, and are almost ex-

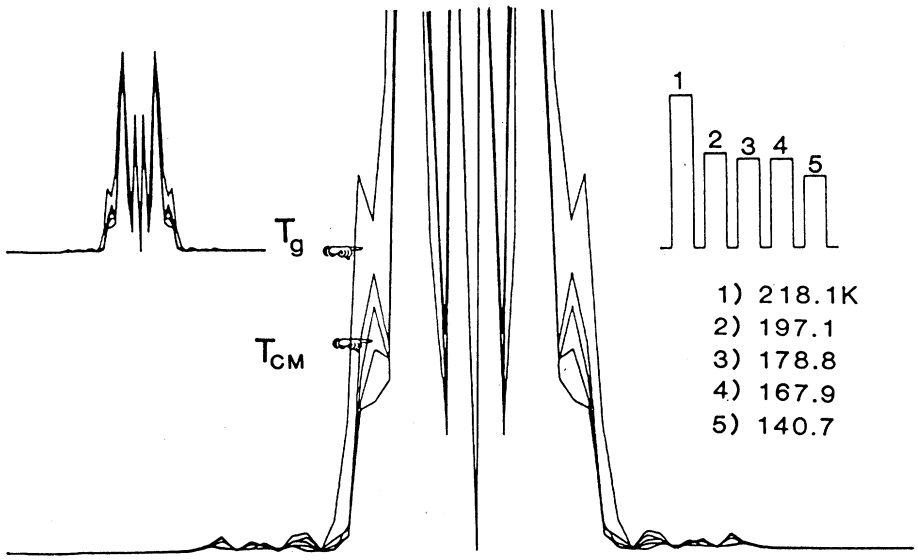

FIG. 12. Autocorrelation functions of some D-Tempone and MBBA low-temperature spectra are plotted coincidently to the same scale. Center diagram is an enlargement of the inset diagram in the upper left. Higher-frequency component lines are seen to decrease in relative height below the main glass and chain-melting transition temperatures. Here, 1 shows an above-T_g spectra, while 2 and 3 are below the transition, yet above the chain-melting transition. The rigid-limit spectrum is shown in 5. Inset at the upper right shows the relative scaling factor of each spectrum. The glass transitions appear both in the frequency distribution of the power-density spectra, and the overall power absorbed, as may be seen from the inset.

clusively dominant in slow-tumbling glassy and rigid-limit spectra. A more general discussion of the use of power-spectrum analysis may be found in Ref. 18.

Some easily observed trends may be noticed. First, the spectral distribution shifts from higher frequencies to lower frequencies with lowered temperature demonstrating that as T is decreased η and τ are increased. This is just reflecting the observation that a slower-tumbling probe molecule will produce a wider absorption peak. Approaching the glass transition, one notices the setting in of a powder power-density spectrum, corresponding to the powder pattern observed in the derivative absorption signal. There is a sudden decrease in absorbed power at the main glass transition T_g for both probes, reflecting the intensity results about which we have already commented. Lowered temperatures result in the elimination of no additional lines from the frequency spectrum, only in shifts of relative magnitude.

In addition to these intensity- and saturation-related glass transition effects observable in the power-density spectra, one finds another glass transition indicator in both the 0° and 90° MBBA data that was not present in the isotropic glass previously studied. These autocorrelation functions show the enhanced presence of additional lines marginally present in the glassy spectra as entering in the above T_g supercooled-liquid spectra. These lines are of higher frequency and represent narrower EPR spectral lines and faster molecular tumbling regions. This phenomena is illustrated in Figs. 11 and 12 and presents yet another indicator of the glass transition. One may hypothesize that the larger size and anisotropy of the liquid-crystal molecule, as compared to the isotropic dibutyl phthalate previously studied, supports a more pronounced spectral line-shape change at the glass transition critical temperature.

IV. SUMMARY AND CONCLUSIONS

The major experimental accomplishment discussed in this paper is the development of a multispectra, rapid-sweep mode for gathering EPR spectral data. This has allowed us to observe spectra from the heretofore unobservable supercooled pre-glass-transition regions of nematic liquid-crystalline MBBA. The data observed in this region from both D-Tempone and N-6 probes may be accounted for in light of the Grest-Cohen glass-formation model. We have further extended our earlier[9,18,41] EPR probe molecule studies of the liquid and glass states of some organic glass-forming liquids to include total line-shape determination of liquid-crystalline EPR and material parameters. Both 0° and 90° orientations of the liquid-crystal director tilt axis from the EPR magnetic field were recorded.

Modeling the glass as a phase including two sites of different rotational correlation values, we are able to fit the experimental N-6 probe EPR spectra as a sum of spectral components from each site. Difference spectra of above and below T_g glass transition spectra match closely experimental rigid-limit spectra. The 90° difference spectra produce a nonobservable 90° liquidlike spectrum that may be found through computer simulation. Nonbroadened parallel glassy EPR spectra and increased low-field to high-field splittings in the perpendicular spectra support the two-site glass model.

The glass transition in MBBA was found to occur at considerably faster molecular relaxation times than in isotropic liquids. It is postulated that this may be an effect of greater defect growth in a "2D" glass than in an amorphous isotropic solid. We also investigated the dependence of the signal intensity and the power-frequency spectrum on temperature and phase state.

These further conclusions, both theoretical and experimental, are presented. (1) The Heisenberg spin exchange interaction follows a simple model for the N-6 probe. (2) Cubic splines fitted to the center line peak heights versus temperature accurately predict the glass transition of the D-Tempone probe molecule; these line heights show the main glass transition and the chain-melting transition for the N-6 probe. (3) The onset of the glass phase is also marked with a change to a rigid, almost unchanging, powder pattern for the N-6 probe at the main transition temperature, and for the narrow-lined D-Tempone probe at the chain-melting transition temperature. (4) This is interpreted as a result of a large percentage $(1-p)$ of the cells of the liquid becoming solidlike at T_g, leaving only p cells in a fluidlike medium. (5) The measured τ of the glass is according to the microdiffusion model presented earlier. (6) The experimentally measured liquid-crystalline order parameter S follows the Maier-Saupe theory even into the supercooled and glassy regions of the material. (7) The setting in of the glass-state powder-pattern-like spectrum is also observed in the power-density spectra at T_g and at T_{CM}. (8) A dip in power-density line heights at all frequencies just above the glass-transition temperature T_g is consistent with saturation phenomena and a concurrent decrease in spectral intensity. (9) Measurement of total signal intensity unveils a $1/T$ Curie-law dependence in the low-viscosity region of the liquid, a dependence that is consistent with saturation phenomena in the supercooled liquid, and an apparent reduction of the saturation effect in the glass state. (10) This reduction of the saturation effect could be a result of a decrease in T_1, the spin-lattice relaxation time, brought about from the shift of a large fraction of the material from a liquid to solidlike structure.

Molecular probe studies of ordered glasses allow partial control of some of the degrees of freedom found in amorphous systems. Here they lend valuable evidence useful in understanding the microscopic organization and dynamics of the glass state and glass transition.

ACKNOWLEDGMENTS

We extend our thanks to Dr. Mary Neubert of the Liquid Crystal Institute (LCI) for purifying and crystallizing the deuterated Tempone spin probe, Mr. David Chapman of the Kent State Biology Department for synthesizing this probe, and Dr. Neubert of the LCI for providing the MBBA liquid-crystal samples.

---

*To whom all correspondence should be addressed.

[1]M. Sorai, T. Nakamura, and S. Seki, *Proceedings of the International Conference on Liquid Crystals, Bangalore, India, 1973,* edited by S. Chandrasekhar (Indian Academy of Sciences, Bangalore, 1973).

[2]S. E. B. Petrie, H. K. Bucher, R. T. Klingbiel, and P. I. Rose, Eastman Org. Chem. Bull. **45**, 1 (1973).

[3]N. Kirov, M. P. Fontana, and N. Affanassieva, Mol. Cryst. Liq. Cryst. **89**, 193 (1982).

[4]W. J. LaPrice and D. L. Uhrich, J. Chem. Phys. **71**, 1498 (1979).

[5]D. Todoroff, Ph.D. dissertation, Kent State University, Kent, Ohio, 1983.

[6]R. Marande, Ph.D. dissertation, Kent State University, Kent, Ohio, 1984.

[7]Y. Poggi, R. Aleonard, and J. Robert, Phys. Lett. **54A**, 393 (1975).

[8]S. D. Coren, C. Korn, and S. B. Marks, Phys. Rev. Lett. **34**, 1212 (1975).

[9]J. I. Spielberg and E. Gelerinter, Chem. Phys. Lett. **92**, 184 (1982).

[10]A. E. Stillman, L. L. Jones, R. Schwartz, and B. L. Bales, Liquid Cryst. Ordered Fluids **3**, 399 (1978).

[11]E. Meirovitch, D. Igner, E. Igner, G. Moro, and J. H. Moro, J. Chem. Phys. **77**, 3915 (1977).

[12]C. F. Polnaszek, G. V. Bruno, and J. H. Freed, J. Chem. Phys. **58**, 3185 (1973).

[13]G. S. Grest and M. H. Cohen, in *Advances in Chemical Physics,* edited by Stuart A. Rice (Wiley, New York, 1981), Vol. 48, p. 455.

[14]M. H. Cohen and G. S. Grest, Phys. Rev. B **20**, 107 (1979).

[15]G. S. Grest and M. H. Cohen, Phys. Rev. B **21**, 411 (1980).

[16]P. G. de Gennes, *The Physics of Liquid Crystals* (Oxford University, London, 1974).

[17]J. L. W. Pohlmann and W. Elser, in *Liquid Crystals 2,* edited by G. H. Brown (Gordon and Breach, London, 1969), p. 123.

[18]J. I. Spielberg and E. Gelerinter, Phys. Rev. B **30**, 2319 (1984).

[19]W. E. Shutt, E. Gelerinter, G. C. Fryburg, and C. F. Sheley, J. Chem. Phys. **59**, 143 (1973).

[20]O. H. Griffith, D. W. Cornell, and H. M. McConnell, J. Chem. Phys. **43**, 2909 (1965).

[21]W. L. Hubbell and H. M. McConnell, J. Am. Chem. Soc. **93**, 314 (1971).

[22]J.-C. Hsia, H. Schneider, and I. C. P. Smith, Can. J. Biochem. **49**, 614 (1971).

[23]S. A. Zager and J. H. Freed, J. Chem. Phys. **77**, 3344 (1982).

[24]The authors wish to acknowledge Mr. Peter McCabe for help in taking the N-6 spectra.

[25]J. I. Spielberg, Ph.D. dissertation, Kent State University, Kent, Ohio, 1985.

[26]G. Moro, Cornell University Report, 1980 (unpublished). Programs courtesy of J. H. Freed.

[27]G. Moro and J. H. Freed, J. Phys. Chem. **84**, 2837 (1980).

[28]C. F. Polnaszek and J. H. Freed, J. Phys. Chem. **79**, 2283 (1975).

[29]J. S. Hwang, R. P. Mason, L. P. Hwang, and J. H. Freed, J. Phys. Chem. **79**, 489 (1975).

[30]K. V. S. Rao, C. F. Polnaszek, and J. H. Freed, J. Phys. Chem. **81**, 449 (1977).

[31]S. A. Goldman, G. V. Bruno, C. F. Polnaszek, and J. H.

Freed, J. Chem. Phys. **56**, 716 (1972). Programs courtesy of C. F. Polnaszek.
[32]A. L. Berman, E. Gelerinter, G. H. Brown, and G. C. Fryburg, in *Liquid Crystals and Ordered Fluids, 2* (Chicago, 1973).
[33]J. H. Freed, G. V. Bruno, and C. F. Polnaszek, J. Chem. Phys. **75**, 3385 (1971).
[34]J. H. Freed, in *Spin Labeling Theory and Applications,* edited by L. J. Berliner (Academic, New York, 1976).
[35]M. P. Eastman, R. G. Kooser, M. R. Das, and J. H. Freed, J. Chem. Phys. **51**, 2690 (1969).
[36]M. P. Eastman, G. V. Bruno, and J. H. Freed, J. Chem. Phys. **52**, 2511 (1970).
[37]J. M. Kosterlitz and D. J. Thouless, J. Phys. C **5**, L124 (1972).
[38]D. R. Nelson and B. I. Halperin, Phys. Rev. B **19**, 2457 (1979).
[39]R. J. Birgeneau and J. D. Litster, J. Phys. (Paris) Lett. **39**, L399 (1978).
[40]N. W. Ashcroft and N. D. Mermin, *Solid State Physics* (Holt, Rinehart and Winston, Philadelphia, 1976).
[41]J. I. Spielberg and E. Gelerinter, J. Chem. Phys. **77**, 2159 (1982).
[42]W. J. Line and J. H. Freed, J. Chem. Phys. **83**, 379 (1979).
[43]S. Lee and D. P. Ames, Bull. Am. Phys. Soc. **29**, 492 (1984).
[44]M. Plumley, E. Gelerinter, and J. I. Spielberg, Chem. Phys. Lett. **13**, 299 (1985).
[45]N. M. Atherton, *Electron Spin Resonance* (Wiley, New York, 1973).
[46]Ron Bracewell, *The Fourier Transform and its Applications* (McGraw-Hill, New York, 1965).
[47]E. Oran Brigham, *The Fast Fourier Transform* (Prentice-Hall, Englewood Cliffs, N.J., 1974).
[48]J. S. Bendat and A. G. Piersol, *Measurement and Analysis of Random Data* (Wiley, New York, 1966).
[49]R. C. Singleton, Commun. ACM **10**, 647 (1967).
[50]M. Rance, Ph.D. dissertation, University of Guelf, Ontario, Canada, 1981.